Asian Journal of Chemistry; Vol. 23, No. 9 (2011), 4156-4164

ASIAN JOURNAL OF CHEMISTRY

www.asianjournalofchemistry.co.in

Preparation, Characterization and Luminescence of (MCM-41)-AgBr Nanocomposite Materials

XIAO-DONG LI and QING-ZHOU ZHAI*

Research Center for Nanotechnology, Changchun University of Science and Technology, 7186 Weixing Road, Changchun 130022, Jilin Province, P.R. China

*Corresponding author: Fax: +86 431 85383815; Tel: +86 431 85583118; E-mail: zhaiqingzhou@163.com; zhaiqingzhou@hotmail.com

(*Received*: 23 December 2010; *Accepted*: 23 May 2011) AJC-9989

MCM-41 was used as host for accommodating AgBr into the channels by three methods *i.e.*, heat diffusion, microwave-assisted and ion exchange methods. A series of characterizations were used to characterize the prepared nanocomposites. When the content of AgBr was below 10 wt %, the results showed that the AgBr located in the channels of MCM-41 and the framework of the MCM-41 in the nanocomposites were not destroyed. Analyses of the luminescent properties of the (MCM-41)-AgBr were carried out and the emission peak shifted to the lower energy side with increasing loading density of AgBr, indicating that the AgBr were confined in the channels of MCM-41 and the quantum confinement effect in the AgBr nanoparticles as a consequence of their samll size. The (MCM-41)-AgBr prepared by microwave-assisted method had more intensity than the (MCM-41)-AgBr nanocomposites prepared by other method. The AgBr were successfully incorporated into the channels of MCM-41 and the prepared nanocomposites possessed interesting optical properties.

Key Words: Nanocomposite material, MCM-41 molecular sieve, AgBr.

INTRODUCTION

The study of the physical properties of confined nanomaterials has become a very active field of research in recent years. The reason to investigate such materials is fundamental due to their considerably different properties from those of the corresponding bulk materials. In the meantime, nanoparticles also referred to as quantum dots, have caused enormous attention due to their potential applications in catalysis, semiconductors, magnetic nanocomposite materials, adsorbents, miniaturized electronic and optical devices[1-8]. Since the physical properties depend on both the size and the shape of the nanoparticles, it is important to control size and shape in their syntheses and to arrange them over useful dimensions[9,10]. In contrast to the conventional preparation methods, the use of an inorganic matrix as a host for nanocrystalline particles can provide an effective way of tailoring a uniform size and controlling the homogeneous dispersion of ultrafine clusters[11]. Mesoporous molecular sieves, first recognized by scientists from the Mobil Corporation[12,13], represent a new class of inorganic materials. These new ordered mesoporous materials have stimulated great interest in the scientific community, principally, in the fields of catalysis and materials science[14-19]. The mesoporous MCM-41 material, the most widely studied among the numerous mesoporous materials reported so far, is an amorphous, mesoporous silica material that is principally defined by domains of highly organized hexagonal arrays of one-dimensional, parallel cylindrical channels throughout its structure. The effective pore size of the channels of MCM-41 is tunable through the choice of the templating reactant used in its synthesis, with the effective size controllable from 1.5-10 nm. MCM-41 can be catalysts, adsorbents, *etc*. and have potential practical performance[20-23]. Therefore, studies on MCM-41 are of great interest. On the other hand, metal and semiconductor nanoparticles have increasingly attracted the attention in recent years due to their outstanding and unique size-dependent properties associated with quantum effects. This type of nanoparticles is currently acknowledged for their distinguished performance in optical, electronic and magnetic applications[24]. In the last decades, nanometer silver halide has been the subject of intensive research due to their novel structural, electrical and optical properties different from bulk silver halides[25-27]. Besides its technological significance, silver halide is an important material from scientific point of view since it can be considered as an ideal model system for studying the physical properties of nanometer particles. However, these properties significantly depend on the medium in which nanoparticle silver halide is embedded and depend on the mode of preparation and on the type of carrier used. Silver bromide is a photon processing material essential to the photographic

process and is of practical interest[28]. The size distribution and dispersion of semiconductor AgBr nanoparticles are critical to their performance. So far, several procedures for the preparation of nanostructured silver bromide in various zeolite molecular sieves[29-31]. Mesoporous materials have been suggested as ideal hosts to form ordered and well dispersed semiconductor AgBr nanocomposite due to their periodic and size-controllable pore channel (2-10 nm) and high surface areas. Also, mesoporous materials have been regarded as "nano-reactors" due to the strong localized fields within the channels[32-34]. Properties of semiconductor AgBr nanoparticles are determined not only by the confinements of the host material but also by the properties of the host material, which offer a means of manipulating the desirable performance of the material. Recently, Hamal *et al*.[35], reported that the high-surface area AgX-SiO_2 (X = Cl, Br, I) photacatalysts were synthesized by using hexadecyltrimethyl ammonium bromide as structure-directing template and the photoactivities of silver halide-silica photocatalyst system in both gas-phase (rhodamine B degradation) under light irradiation were also investigated. Additionally, AgBr[36] was dispersed on an Al-MCM-41 support and was studied as a visible-light photocatalyst for the decomposition of acetaldehyde in the gas phase. However[36], some metal ions can be incorporated within framework of the MCM-41 during the co-assembly process and the long-range order of the final product can be lowered during the synthesis. The key drawback associated with these methods[35,36] is the difficulty in controlling the location of the growth of nanoparticles and preventing their uncontrolled aggregation on external surfaces of MCM-41. Nanometer MCM-41 is a novel mesoporous molecular sieve prepared by Cai *et al*.[37]. In this work, we report our results to illustrate that the nanometer MCM-41 can be used as host to synthesize nanosized AgBr in its channels by three methods *i.e.*, solid-phase thermal diffusion, microwave diffusion and ion exchange methods. The as-prepared (nanometer MCM-41)-AgBr samples were characterized by a series of methods including powder X-ray diffraction (XRD), Fourier transform infrared spectroscopy (FT-IR), low-temperature nitrogen adsorption-desorption technique at 77 K, high resolution transmission electron microscopy (HRTEM), scanning electron microscopy (SEM) and luminescence studies. The combined experimental results demonstrate that the well-dispersed AgBr particles were mostly confined in the channels of the nanometer MCM-41, the prepared nanocomposite materials show the properties of luminescence.

EXPERIMENTAL

Cetyltrimethylammonium bromide (CTMAB, Changzhou Xinhua Research Institute for Reagents, China), tetraethyl orthosilicate (TEOS, Sinopharm Chemical Reagent Co. Ltd., China), sodium hydroxide (Beijing Chemical Reagent Plant, China), sliver bromide (Shanghai Jingchun Chemical Reagent Comapany, China), sliver nitrate (Beijing Chemical Reagent Plant, China). All reagents used in the experiment were analytical grade. Deionized water was used throughout the experiments.

Syntheis of MCM-41: MCM-41 molecular sieve was prepared according to the reported procedure[37]. Under the basic condition, the CTMAB was used as a template and TEOS was used as the structure-directing agent. 1.0 g of CTMAB was added to 480 mL of deionized water at 80 ºC under vigorous stirring until its complete dissolution, followed by addition of 3.5 mL of NaOH (2 mol L^{-1}). Then 5 mL of TEOS was added dropwise to the above solution under vigorous stirring. The mixture was strirred for 2 h at 80 ºC. The resulting product was filtered, washed with deionized water for three times and dried in air at room temperature. The white powder was calcined at 550 ºC for 4 h to decompose the surfactant. The prepared powder was MCM-41.

Preparation of (MCM-41)-AgBr host-guest nanocomposite materials: The typical preparation of (MCM-41)-AgBr host-guest nanocomposites including three methods: (a) the MCM-41 was used as the host to produce the (MCM-41)-AgBr host-guest nanocomposites. Firstly, the MCM-41 was dehydrated at 300 ºC for 2 h to ensure the removal of the adsorbed water and then mixed with AgBr in different weight ratio (5 and 10 wt %). The mixtures were heated at 350 ºC for 36 h. Finally, the samples were cooled down to room temperature in an oven and stored in darkness. The samples were designed as S1 and S2 (solid-phase thermal diffusion method); (b) similarly, the MCM-41 was dehydrated at 300 ºC for 2 h to ensure the removal of the adsorbed water and then mixed with AgBr in different weight ratio (5 and 10 wt %). The mixtures were irradiated by microwave for 10 min at 750 W in a microwave oven. Then, the samples were cooled down to room temperature in the oven and stored in darkness. The samples were designed as S3 and S4 (microwave diffusion method); (c) the mixture of MCM-41 and $AgNO_3$ aqueous solution with different concentration (0.13 and 0.26 mol/L) was stirred for 24 h at room temperature. The solution was then centrifuged and the supernatant aqueous solution decanted. The residue was washed 3 times with water to remove Ag^+ from the external surface and then dried in air. 0.025 or 0.050 g KBr and an appropriate amount of the above dried solid particles were mixed in 30 mL of deionized water. The mixed solution was stirring at 50 ºC for 12 h, then the resulting products were filtered and washed with water. The obtained solid samples were dried and calcined at 250 ºC for 3 h in darkness. The products were designated as S5, S6 (ion exchange method).

Characterization: Determination of AgBr was made by atomic absorption spectrometry with Hitachi Z-8000 polarization Zeeman atomic absorption spectrophotometer. Powder X-ray diffraction (XRD) patterns were obtained on a Bruker D8/Advance diffractometer with CuK_α radiation (40 kV, 60 mA). For the low angle XRD, the 2θ scans covered the range of 1-8º with a step of 0.02º, whereas for the wide angle XRD, the 2θ scans covered the range of 10-70º with a step of 0.06º. Fourier transform infrared spectroscopic (FT-IR) results were measured with a Nicolet 5DX-FTIR spectrometer within the wavenumber range 4000-400 cm^{-1} using KBr pressed pellet technique (99 wt. % of KBr). The pore diameter, the pore volume and specific surface area were determined with low temperature nitrogen adsorption and desorption technique at 77 K using a Micromeritics ASAP 2020 V3.01 H analyzer (The

American Mike Company). The data were calculated in terms of the model of Bdb (Broekhoff and de Boer) method[38]. The surface area was calculated by the Brunauer-Emmett-Teller (BET) method[39] and the pore size distributions were evaluated from the adsorption branches of the nitrogen isotherms using the Barrett-Joyner-Halenda (BJH) model[40]. High resolution transmission electron microscopy (HRTEM) of a sample deposited on carbon-copper grids was performed using a FEI Tecnai G2 F20 field-emission transmission microscope (Netherlands) operating at 200 kV. Scanning electron microscopy (SEM) images were taken on a PHILIPS XL30 field-emission environmental scanning electron microscope (Netherlands) instrument. The excitation and emission spectra were carried out at room temperature with a Hitachi F-7000 spectrophotometer (Japan) equipped with a 150 W xenon lamp as the excitation source.

RESULTS AND DISCUSSION

Chemical analysis: The contents of AgBr in all samples were obtained by atomic absorption spectrometry. Their percentages were 4.76 % for S1, 4.76 % for S2, 4.76 % for S3, 9.09 % for S4 and 1.73 % for S5 in mass, indicating the AgBr has been in the (MCM-41)-AgBr nanocomposite materials.

Powder X-ray diffraction (XRD): Low angle XRD patterns of the synthesized samples are shown in Fig. 1A. All the prepared samples (except S6) show well resolved d_{100} diffraction peaks. The d_{100} spacing value is nearly unchanged before or after AgBr is assembled, indicating no significant loss of sample ordering quality upon introduction of AgBr molecules. In addition, we observed the decrease of the relative reflection intensities of d_{100} peaks as the amount of AgBr introduced into the mesopores of the MCM-41 host is increased. This indicates the reduction of the ordered degree of MCM-41 host due to the incorporation of AgBr. MCM-41 (Fig. 1A-a) gives four well-resolved peaks that can be indexed as (100), (110), (200), (210) diffraction peaks associated with p6mm hexagonal symmetry[37]. In contrast, only (100), (110) diffraction peaks are detected in the XRD patterns of the (MCM-41)-AgBr samples (except S6) and higher order Bragg reflections of the hexagonal structure are not resolved, suggesting that the structures of (MCM-41)-AgBr are more disordered as compared with that of MCM-41. The disappearance of the diffraction peaks for S6 (Fig. 1A-g) demonstrated a disordered mesostructure, indicating that the collapse of the mesostructure took place due to the agglomeration of crystalline particles of AgBr.

The wide angle X-ray powder diffraction patterns of the samples were recorded in Fig. 1B. As observed in Fig. 1B, the XRD peaks are characteristic of nanometer MCM-41 (Fig. 1B-a) and AgBr (Fig. 1B-b) structures. The XRD reflections of AgBr completely disappeared (Fig. 1B-c) in the sample S1, showing that the AgBr particles by heat diffusion (350 ºC) were highly dispersed in the mesoporous channels when their loading was about 5 wt %. Such phenomena also have been observed in samples S3 (Fig. 1B-e) and S5 (Fig. 1B-g). It indicated that the guest AgBr exists inside the pore channels of the host MCM-41 molecular sieve when AgBr loading is low. Similar results were reported by previous workers[27,41]. However, the peaks of AgBr appeared when the content of crystalline AgBr in samples S2, S4 with 10 wt % AgBr loading (Fig. 1B-d, f).

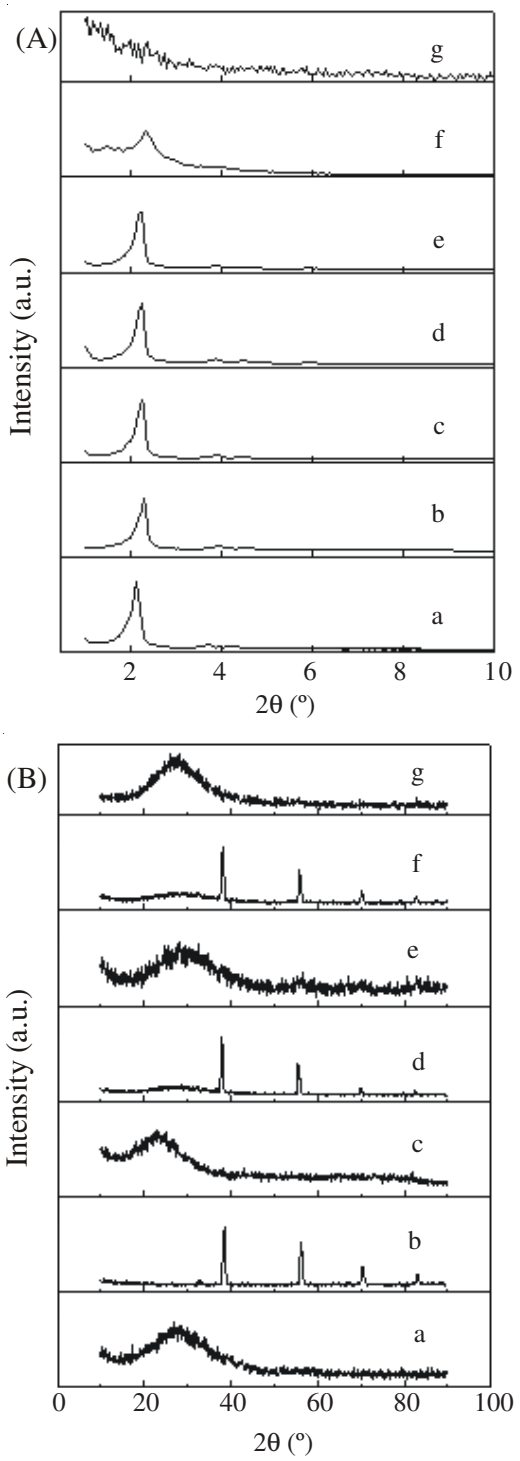

Fig. 1. (A) Small-angle XRD patterns of: (a) nanometer MCM-41, (b) S1 [(nanometer MCM-41)-AgBr with 5 wt % AgBr, heat diffusion at 350 ºC], (c) S2 [(nanometer MCM-41)-AgBr with 10 wt % AgBr, heat diffusion at 350 ºC], (d) S3 [(nanometer MCM-41)-AgBr with 5 wt % AgBr, microwave diffusion method], (e) S4 [(nanometer MCM-41)-AgBr with 10 wt % AgBr, microwave diffusion method], (f) S5 [(nanometer MCM-41)-AgBr with 5 wt % AgBr, ion exchange method], (g) S6 [(nanometer MCM-41)-AgBr with 10 wt % AgBr, ion exchange method]. Fig. 1(B) wide-angle XRD pattens of: (a) nanometer MCM-41, (b) AgBr, (c) S1 [(nanometer MCM-41)-AgBr with 5 wt % AgBr, heat diffusion at 350 ºC], (d) S2 [(nanometer MCM-41)-AgBr with 10 wt % AgBr, heat diffusion at 350 ºC], (e) S3 [(nanometer MCM-41)-AgBr with 5 wt % AgBr, microwave diffusion method], (f) S4 [(nanometer MCM-41)-AgBr with 10 wt % AgBr, microwave diffusion method], (g) S5 [(nanometer MCM-41)-AgBr with 5 wt % AgBr, ion exchange method]

Fourier transform infrared spectra can reflect the change of configuration of the framework of molecular sieve host after incorporation of guest into molecular sieve. Fig. 2 shows the FT-IR spectra of the samples over the region of 4000-400 cm^{-1}. There is no obvious peaks of AgBr in Fig. 2a. In the spectrum of MCM-41(Fig. 2b), the bands at 3435 and 1637 cm^{-1} attributed to the stretching vibration of hydroxyl groups and to the deformation vibration of water can be observed, respectively. The band at 960 cm^{-1} is attributed to the Si-OH stretching vibration. The peak at 1080 cm^{-1} corresponds to the asymmetric stretching vibration of Si-O-Si and the bands at 800 and 470 cm^{-1} can be assigned to the symmetric stretching and deformation modes of Si-O-Si. Compared with the curve b, the FT-IR spectra of the (MCM-41)-AgBr with various preparative methods show six corresponding characteristic peaks of the MCM-41. This indicates that the MCM-41 frameworks in the (MCM-41)-AgBr are still remained intact. However, the peak intensities of the (MCM-41)-AgBr samples are lower than that of the MCM-41 and the positions of these peaks shifting towards the lower wavenumber can be considered as an indication for the incorporation of AgBr into the pores of the MCM-41. The intensity of the band centered at 960 cm^{-1} for (MCM-41)-AgBr is apparently lower than that for MCM-41. It may be because an interaction of the AgBr with the silica surface, which led to less adsorption of hydroxyl group[42]. Therefore, the majority of AgBr was incorporated into the channels of the MCM-41 molecular sieve.

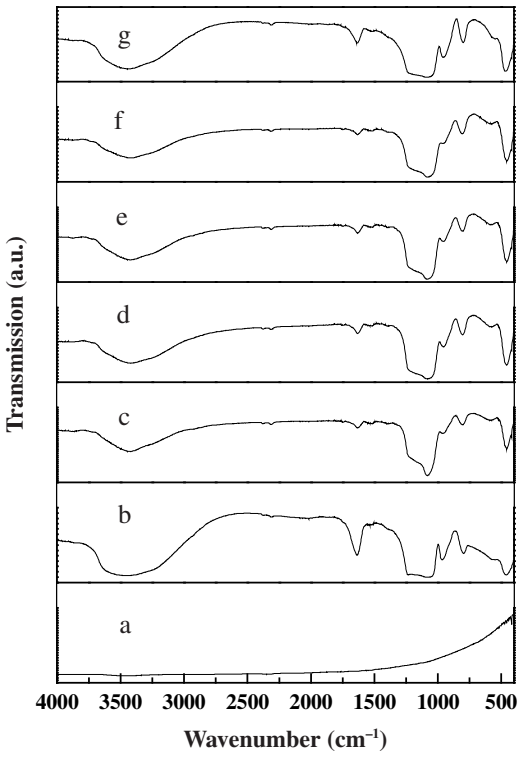

Fig. 2. Infrared spectra of each sample: (a) AgBr, (b) nanometer MCM-41, (c) S1 ((nanometer MCM-41)-AgBr with 5 wt % AgBr, heat diffusion at 350 ºC), (d) S2 ((nanometer MCM-41)-AgBr with 10 wt % AgBr, heat diffusion at 350 ºC), (e) S3 ((nanometer MCM-41)-AgBr with 5 wt % AgBr, microwave diffusion), (f) S3 ((nanometer MCM-41)-AgBr with 10 wt % AgBr, microwave diffusion), (g) S5 ((nanometer MCM-41)-AgBr with 5 wt % AgBr, ion exchange process)

Low-temperature nitrogen adsorption-desorption isotherm: Nitrogen physisorption is a technique to assess the textures of porous materials. The nitrogen adsorption-desorption isotherms of the samples and the corresponding pore size distribution curves calculated using BJH method are depicted in Fig. 3. Consistent with the XRD results, the (nanometer MCM-41)-AgBr samples (except S5) give similar isotherm curves to that of parent MCM-41, which reflects the maintenance of ordered mesostructures. According to the IUPAC classification, all isotherms are of type Langmuir IV with a typical H1 hysteresis loop[43,44], which indicates that the samples have mesoporous channels and narrow pore size distributions. All samples show typical type IV isotherm with two regions of strong N_2 uptake. There are two hysteresis loops in both regions. The one at low relative pressure ($0.3 < P/P_0 < 0.4$) indicates the uniformity of the mesoporous size distribution and the other that occurs at $P/P_0 > 0.8$ corresponds to capillary condensation within interparticle pores. This indicates the filling of the pores with AgBr without damaging the mesoporosity. At the beginning of Fig. 3A-a, 3A-b and 3A-c, the nitrogen uptakes increase slowly at the relatively lower pressure ($P/P_0 < 0.3$) due to the monolayer-multilayer adsorption of nitrogen on the pore walls. When the relative pressure is $0.3 < P/P_0 < 0.4$, the isotherm of nanometer MCM-41 and the prepared materials displayed the sharp increase on the adsorption isotherms, being characteristic of capillary condensation within the uniform mesopores of the nanometer MCM-41. However, such characteristic gradually becomes weak in sample S5 (Fig. 3A-d, loading AgBr by ion exchange method), indicating that the partial blockage or collapse of the meso-channels occurred during the AgBr loading. At relatively high pressures ($P/P_0 > 0.4$), a gentle plateau and a sharp rise could be observed, which is associated with multilayer adsorption of N_2 on the surface of the pore channels and N_2 uptake filling all other available pores, respectively. Simultaneously, the N_2 adsorption isotherms from all samples are quite similar to that from MCM-41, while the inflection positions slightly shifted toward lower P/P_0 value and the overall N_2 adsorption amounts decreased depending on the AgBr loading. This is in contrast to the microwave diffusion and solid-phase thermal diffusion methods, the channel space of S5 became inaccessible when AgBr was loaded *via* ion exchange method. It suggests that the AgBr forms plugs rather than dispersed into the pores. These channels which are no longer accessible to N_2 must be filled with AgBr. They could be partially filled with a tiny amount of AgBr. Furthermore, the narrow pore size distributions are observed for all samples in Fig. 3B. Interestingly, a decrease in the mesopore size is noticed with AgBr loading. Such a trend may correspond to an increase in wall thickness of MCM-41 in the(MCM-41)-AgBr with different synthesis methods. The structure information about the samples derived from nitrogen desorption data are listed in Table-1. It shows that the introduction of AgBr leads to a dramatic decrease in the BET surface area and total pore volume.

For calculating the blockage effect of AgBr on the channels of the MCM-41 molecular sieve quantitatively, in this study the normalized surface area of materials (NSA)[45] was calculated. According to the NSA value of material the state of guest in the composite materials can be determined as follows[45]:

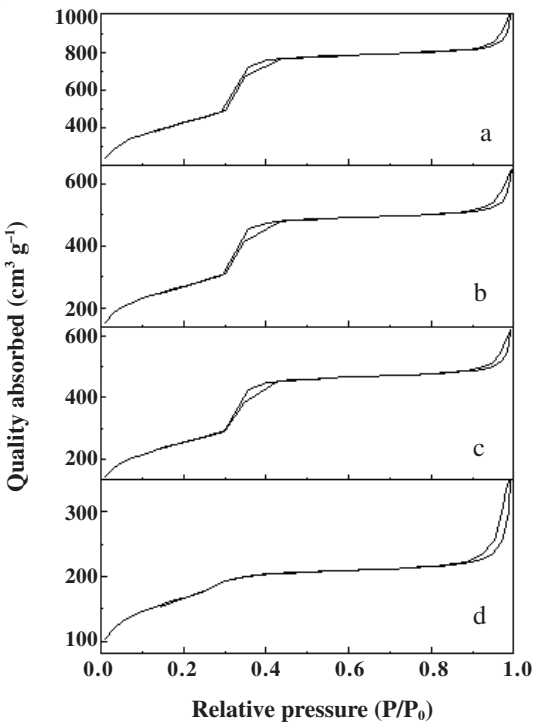

(A)

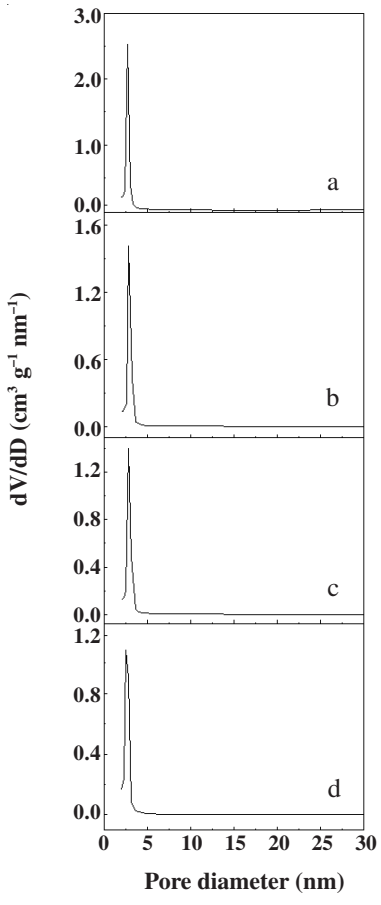

(B)

Fig. 3. (A) Low temperature nitrogen adsorption-desorption isotherms and (B) pore size distribution patterns of samples: (a) nanometer MCM-41, (b) S1 [(nanometer MCM-41)-AgBr with 5 wt % AgBr, heat diffusion at 350 ºC], (c) S3 [(nanometer MCM-41)-AgBr with 5 wt % AgBr, microwave diffusion method], (d) S5 [(nanometer MCM-41)-AgBr with 5 wt % AgBr, ion exchange method]

TABLE-1
PORE STRUCTURE PARAMETERS OF SAMPLES

Sample	d_{100} (nm)	a_0* (nm)	BET surface area (m^2/g)	Pore volume** (cm^3/g)	Pore size*** (nm)
Nanometer MCM-41	3.34	3.85	1329	1.33	3.55
S1	3.85	4.44	946	0.84	3.48
S3	3.92	4.52	894	0.80	3.52
S5	3.75	4.33	587	0.39	2.63

*$a_0 = \frac{2}{\sqrt{3}} d_{100}$. **BJH adsorption cumulative volume of pores.

***Pore size calculated from the adsorption branch.

(1) When the NSA of composite material is <<1, the guest material will form relatively larger particles (Fig. 4a). These particles enter the channels of the molecular sieve, blocking the channels, making the pore volume, surface area and pore size of molecular sieve dramatically smaller. (2) When the NSA of composite material is approximately equals to 1, the guest material will form a non-crystal layer, closely covering the inner surface of the molecular sieve (Fig. 4b). Because these particles attached to the inner surface of the molecular sieve form a new surface, it only covers the original surface. Thus, the NSA value of this type is close to 1. (3) When the NSA of composite material is > 1, the guest material will become very small nanocrystals. It disperses on the internal and external surface of the molecular sieve (Fig. 4c), because the size of these nanocrystals is very small, making a significant increase of surface area in the composite material. So the NSA is much larger than 1.

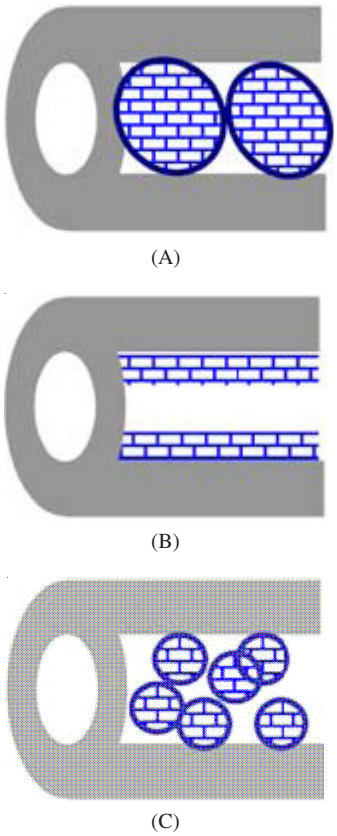

(A)

(B)

(C)

Fig. 4. Guest phase assembling inside the MCM-41. (A) type I; (B) type II; (C) type III[45]

The formula of normalized surface area (NSA) is as follows[45]:

$$NSA = \frac{SA_1}{1-y} \times \frac{1}{SA_2}$$

SA_1 and SA_2 are the surface area of (MCM-41)-AgBr nanocomposite materials and the original MCM-41 molecular sieve powder, respectively, y is mass fraction of the AgBr in the composite material.

In the present study, the NSA values of the S1, S3 and S5 samples are 0.75, 0.71 and 0.50 from the NSA values of the samples. We can see that the NSA values of S1 and S3 samples are approximate to 1. Therefore, AgBr particles formed a non-crystal layer in the (MCM-41)-AgBr samples. This made pore volume, surface area and pore size of the molecular sieve smaller. These results and the nitrogen adsorption-desorption isotherms results were consistent. However, the NSA value of S5 sample is 0.50, indicating a mass of AgBr nanoparticles incorporated into the channels of the MCM-41 and partly blocked the pores of the MCM-41.

High resolution transmission electron microscopy images: High resolution transmission electron microscopy (HRTEM) images provides a direct observation of the morphology and distribution of AgBr nanoparticles in (nanometer MCM-41)-AgBr with the electron beam parallel (Fig. 5A-a, Fig. 5B-a, Fig. 5C-a and Fig. 5D-a) and perpendicular to the pore channels (Fig. 5A-b, Fig. 5B-b, Fig. 5C-b and Fig. 5D-b). Fig. 5A shows the typical HRTEM images of MCM-41. MCM-41 has a highly ordered honeycomb-like pore array structure and the nanosized channels (about 3-5 nm) can be consistently seen. Fig. 5B, Fig. 5C and Fig. 5D show the HRTEM images of S1, S3 and S5. The HRTEM images of (MCM-41)-AgBr samples in Fig. 5 show well-ordered hexa-gonal arrays of mesopore with one-dimensional channels that is a mesoporous structure of 2-D hexagonal (p6mm). The introduction of AgBr particles does not alter the regular hexagonal array of mesopores. No bulk aggregation of the AgBr on the outer surface could be found, which indicates that the AgBr nanoparticles are confined to the pores of the MCM-41. The pore channels are still open. The AgBr quantum dots inside MCM-41 channels were formed. The formation of AgBr quantum dots can be due to low nucleation rate and the size confinement of pore channels.

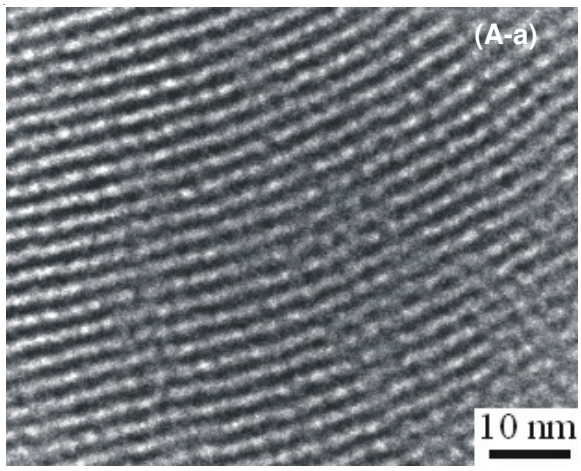

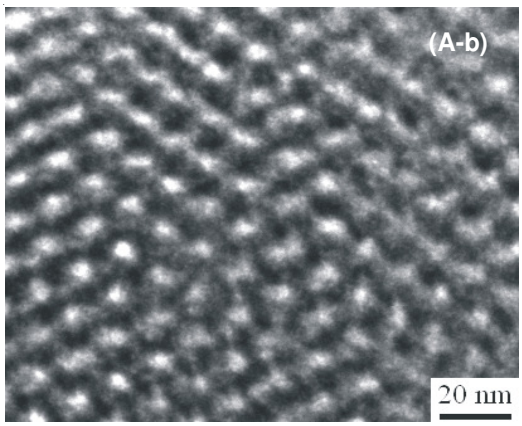

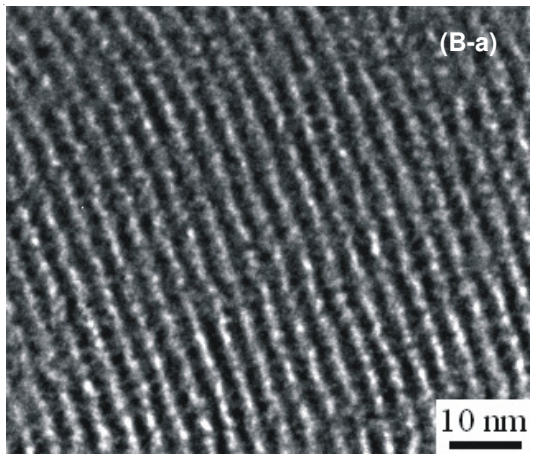

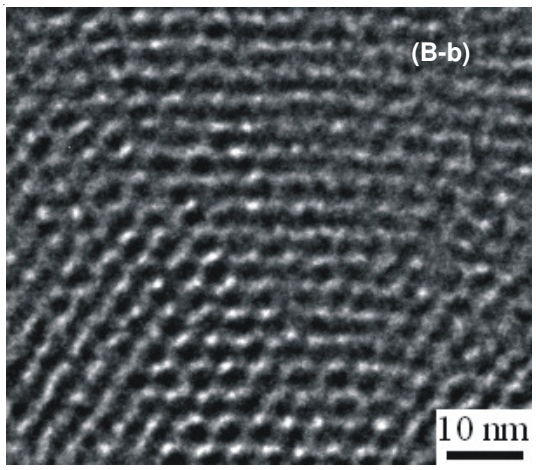

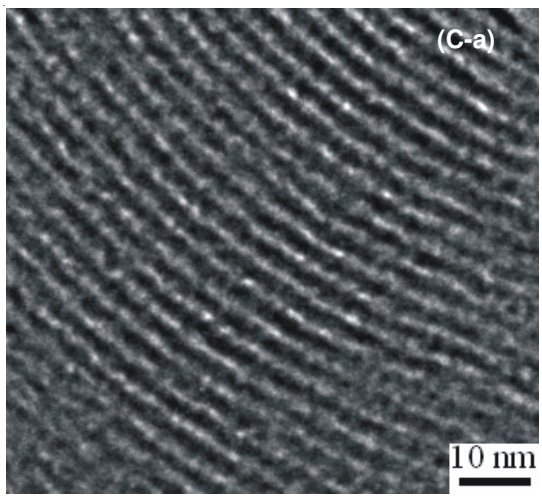

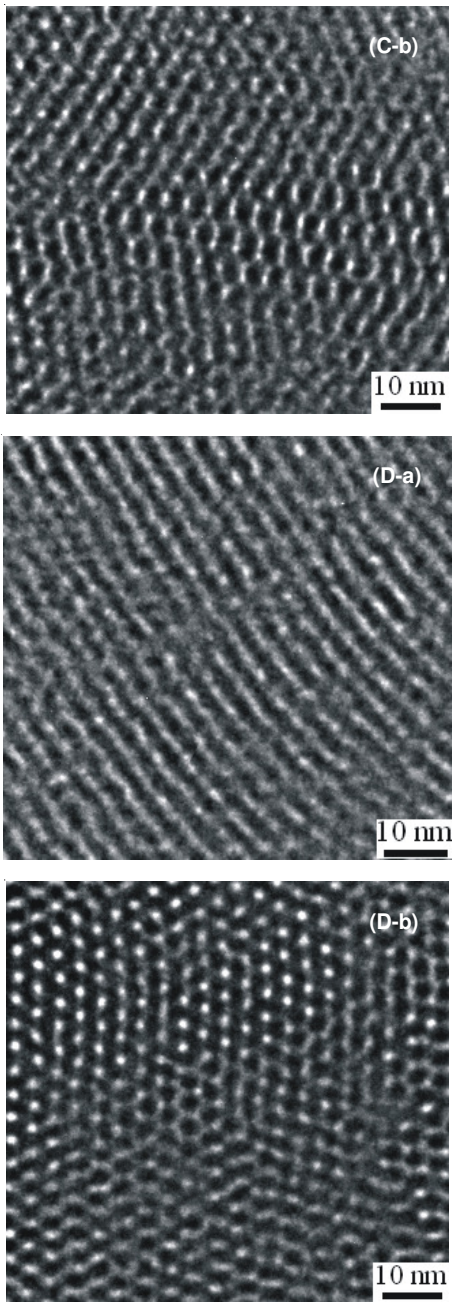

Fig. 5. TEM images of: (A) nanometer MCM-41, (B) S1 [(nanometer MCM-41)-AgBr with 5 wt % AgBr, heat diffusion at 350 ºC], (C) S3 [(nanometer MCM-41)-AgBr with 5 wt % AgBr, microwave diffusion method], (D) S5 [(nanometer MCM-41)-AgBr with 5 wt % AgBr, ion exchange method]

Scanning electron microscopy images: The SEM images reveal the particle morphology and sizes of the (nanometer MCM-41)-AgBr samples. Fig. 6A shows SEM image of the MCM-41 where small spherical particles of mesoporous MCM-41 with diameters of 80-140 nm are evident. Fig. 6B clearly reveals the SEM images of S1 sample synthesized by the solid-phase thermal diffusion method. These particles were made up of rounded shapes which in some cases exhibit hexagonal features. The morphology of the S3 sample (Fig. 6C) seem to globose compared to that of the parent MCM-41 in spite of an increase of the diameter due to AgBr particle incorporation. The AgBr particles should be homogenously distributed in the pore channels of nanometer MCM-41 in the case of the low Ag/Si ratio. Evaluation of the globose particle sizes in Fig. 6C exhibited on average a diameter of 120 ± 10 nm. The S5 sample synthesized by ion exchange method consisited of aggregates of spherical particles, but the individual sphere as small as 120 ± 10 nm is detected as well (Fig. 6D).

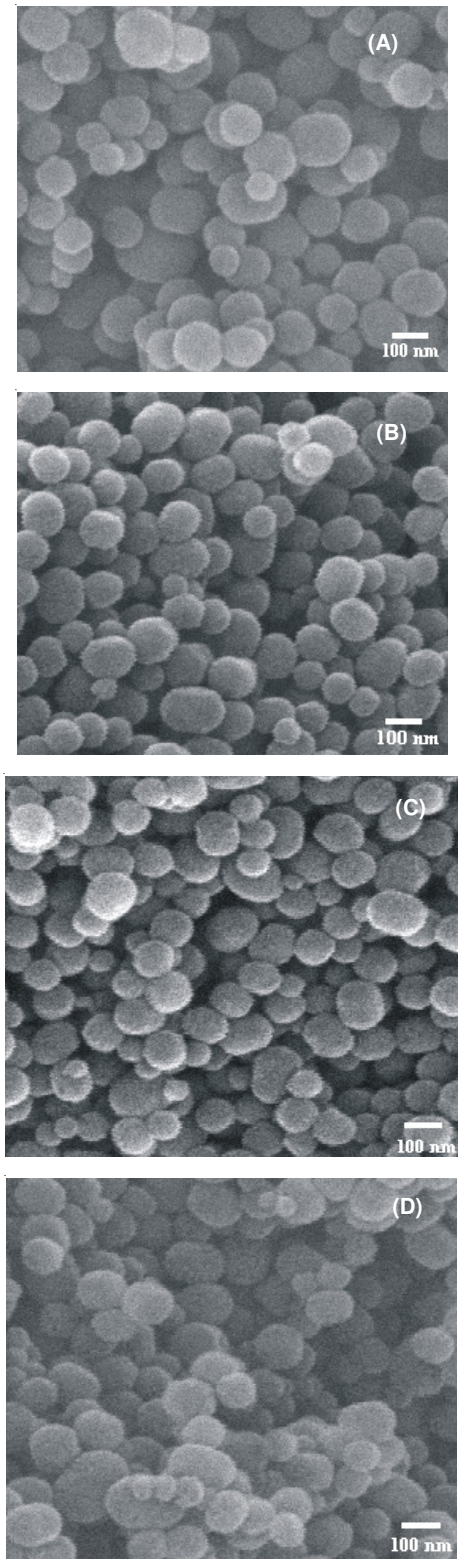

Fig. 6. SEM images of: (A) nanometer MCM-41, (B) S1 [(nanometer MCM-41)-AgBr with 5 wt % AgBr, heat diffusion at 350 ºC], (C) S3 [(nanometer MCM-41)-AgBr with 5 wt % AgBr, microwave diffusion method], (D) S5 [(nanometer MCM-41)-AgBr with 5 wt % AgBr, ion exchange method]

Luminescence: The luminescence spectra of the samples are shown in Fig. 7. There are no phenomena of luminescence of MCM-41 molecular sieve. However, for the prepared (MCM-41)-AgBr nanocomposite materials, the phenomena of luminescence appeared. As shown in Fig. 1, the frameworks of MCM-41 were not destroyed by the incorporation of the AgBr particles (except S6). This behaviour is consistent with relationship between the quantum confinement theory and the size of the semiconductor particle. Namely, the samller size semiconductor particle has a larger excitation energy. Due to quantum confinement effect of guest inside the matrix, such structure shows optical properties as observed for indirect-band gap semiconductors. Quantum confinement refers to the changes in the physical and optical properties of materials that arise upon size restriction[46,47]. The size regime in which it is appropriate to start to consider these effects is one where the bulk band properties of the material are retained but are modified by the limited spatial extent of the material[48-51]. In very small crystals the confinement effects dominate and a "particle in a box" approach is appropriate. Otherwise, the AgBr nanoparticles show significant quantum size effect (such as energy band discreteness, band gap broadening, blue shift in spectra, *etc*.) as sizes of AgBr nanoparticles are smaller than Bohr radis of exciton of bulk AgBr. Hence, the excitation and emission peaks of (MCM-41)-AgBr shifted toward higher energy with decreasing size of the AgBr nanopaticles. The emission showed the strongest intensity in the (MCM-41)-AgBr nanocomposites prepared by the microwave diffusion method with AgBr loading with 5 wt %. A much weak emission peak shows at 422 nm for the mechanical mixture of MCM-41 and AgBr (5 wt %), which corresponds to the AgBr located on the external surface of MCM-41 (Fig. 7b). The excition peak of the mechanical mixture of MCM-41 and AgBr (5 wt %) is almost not affected by the MCM-41, however, the corresponding excition peaks of (MCM-41)-AgBr moved to the low wavenumber. The group state of AgBr clusters for the mechanical mixture of MCM-41 and AgBr (5 wt %) are not excited to its excited state under the excitation of 422 nm compared with that of (MCM-41)-AgBr nanocomposites. The excitation-emission spectra of S3 (Fig. 7e) show that the emission peaks at 421 nm corresponds to the excitation bands at 209 nm and the excitation energy of the bands increased obviously compared with that of AgBr. This shows that the channels of MCM-41 have stereoscopical confinement effect on the guest AgBr particles. As the stereoscopical confinement effect of MCM-41 made the interaction of Coulomb static electricity between the electrons and the holes enhance. The excitons could be formed. It is considered that the trapping of the electrons is a very fast process and the excitons are not free. As soon as the carriers were captured, they released to the ground state by non-radiative recombination or they recombined and emitted excited photons. The mutual competition of the processes determined the type of the emissions observed. It is observed and theoretically calculated that the luminescence from the indirect exciton of AgBr microcrystals shifts its energy to the higher energy side and increases its intensity as their sizes decrease[52-55]. The luminescence originates from the recombination of the electron and the hole. The strong oscillator strength is from the direct electronic transition

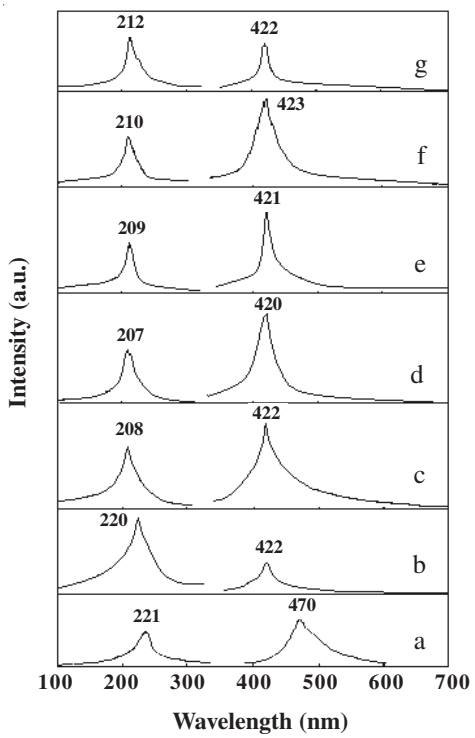

Fig. 7. Luminescence spectra of: (a) AgBr, (b) mechanical mixture of MCM-41 and AgBr (5 wt %), (c) S1 [(nanometer MCM-41)-AgBr with 5 wt % AgBr, heat diffusion at 350 ºC], (d) S2 [(nanometer MCM-41)-AgBr with 10 wt % AgBr, heat diffusion at 350 ºC], (e) S3 [(nanometer MCM-41)-AgBr with 5 wt % AgBr, microwave diffusion method], (f) S4 [(nanometer MCM-41)-AgBr with 10 wt % AgBr, microwave diffusion method], (g) S5 [(nanometer MCM-41)-AgBr with 5 wt % AgBr, ion exchange method]

between the valence state and the conduction state. Apparently, it seems that there is a very weak quantum confinement effect on the photoexcited state of the AgBr microcrystal compared to the bulk. We can qualitatively consider the behaviour of the excitation energy of the microcrystal (E*) compared to the energy of the inter-band transition (E_g) in bulk under an effective mass approximation. According to Brus' theory[56], the energy shift ΔE (= E* – E_g) can be described as:

$$\Delta E = E^* - E_g = \frac{\hbar^2\pi^2}{2R^2}\left(\frac{1}{m_e}+\frac{1}{m_h}\right) - \frac{1.8e^2}{\varepsilon R} \qquad (1)$$

where R is the radius of the microcrystal which is samaller than the exciton Bohr radius, m_e and m_h are the effective masses of the conduction electron and the valence hole, respectively and ε is the dielectric constant of the bulk crystal. In eqn. 1, the image charge effect is not included for simplicity. The first term describes an enhancement of kinetic energies of the electron and the hole. The second term, which reduces the blue shift, is due to the Coulomb attractive force between the electron and the hole. If the mass of the hole has a negative value, ΔE does not increase so much by the first term.

The luminescence of S2 and S4 (Fig. 7 d and f) was relatively weak, which shows that the non-radiative process was very strong and the defects and the surface states of the nanoguests in the channels were very high. From the point of the size of the guest AgBr, the inhomogeneous size was another factor that results in the weak emission or broad bands of this kind of materials. Furthermore, hydroxyl groups of the MCM-41

act as passivation contacts for the stabilization of AgBr nanoparticles in the channels of the MCM-41.

Conclusion

The (MCM-41)-AgBr host-guest nanocomposite materials were successfully synthesized by heat diffusion, microwave-assisted and ion exchange methods. At the same time, incorporation of AgBr in the MCM-41 was successfully carried out for the first time by microwave-assisted synthesis method. The structure and properties of the prepared nanocomposites have been evaluated by XRD, FT-IR, low-temperature nitrogen adsorption-desorption at 77 K, HRTEM, SEM and luminescence study. The results showed that the guest AgBr was highly dispersed in the channels of MCM-41 and no longer existed in the crystalline state when the guest loading was below 10 wt %. When AgBr content exceeded this value, the excess AgBr existed in the form of nanoparticles. In addition, a blue shift on emission peaks of (MCM-41)-AgBr nanocomposites as well as the intensities of emission peaks increased compared to that of AgBr bulk. The blue shift is due to the reason that the channels of MCM-41 have a quantum confinement effect on the AgBr. Furthermore, the (MCM-41)-AgBr prepared by microwave-assisted method has more luminous intensity.

REFERENCES

1. X.-Y. Hao, Y.-Q. Zhang, J.-W. Wang, W. Zhou, C. Zhang and S.-X. Liu, *Micropor. Mesopor. Mater*., **88**, 38 (2006).
2. M.-Z. Cai, Q.-H. Xu and J.-C. Sha, *J. Mol. Catal. A: Chem*., **272**, 293 (2007).
3. E.A. Turner, Y.-N. Huang and J.F. Corrigan, *Eur. J. Inorg. Chem*., 4465 (2005).
4. J. Zhu, Z. Konya, V.F. Puntes, I. Kiricsi, C.-X. Miao, J.W. Ager, A.P. Alivisatos and G.A. Somorjai, *Langmuir*, **19**, 4396 (2003).
5. S.V. Kolotilov, O. Shvets, O. Cador, N. Kasian, V.G. Pavlov, L. Ouahab, V.G. Llyin and W. Pavlishchuk, *J. Solid State Chem*., **179**, 2426 (2006).
6. E. Pardo, P. Burguete, R. Ruiz-Garcia, M. Julve, D. Beltran, Y. Journaux, P. Amoros and F. Lloret, *J. Mater. Chem*., **16**, 2702 (2006).
7. H.R. Emamian, A. Honarbakhsh-Raouf and A. Ataie, *J. Nanosci. Nanotechnol*., **10**, 2897 (2010).
8. Y.P. Hsieh, J.-W. Chen. C.-T. Liang and Y.-F. Chen, *J. Lumin*., **128**, 553 (2008).
9. W. Xu, Y.-T. Liao and D.L. Akins, *J. Phys. Chem. B*, **106**, 11127 (2002).
10. I.V. Golosovsky, I. Mirebeau, E. Elkaim, D.A. Kurdyukov and Y.A. Kumzerov, *Eur. Phys. J.*, **B47**, 55 (2005).
11. S. Sohrabnezhad, A. Pourahmd and M.A. Zanjanchi, *J. Iran. Chem. Soc*., **6**, 612 (2009).
12. J.S. Beck, J.C. Vartuli, W.J. Roth, M.E. Leonowicz, C.T. Kresge, K.D. Schmitt, C.T.W. Chu, D.H. Olson, E.W. Sheppard, S.B. Mccullen, J.B. Higgins and J.L. Schlenker, *J. Am. Chem. Soc*., **114**, 10834 (1992).
13. C.T. Kresge, M.E. Leonowicz, W.J. Roth, J.C. Vartuli and J.S. Beck, *Nature*, **359**, 710 (1992).
14. A.P. Wight and M.E. Davis, *Chem. Rev*., **102**, 3589 (2002).
15. S. Shylesh, P.P. Samuel, S. Sisodiya and A.P. Singh, *Catal. Surv. Asia*, **12**, 266 (2008).
16. K. Moller and T. Bein, *Chem. Mater*., **10**, 2950 (1998).
17. A. Sayari and S. Hamoudi, *Chem. Mater*., **13**, 3151 (2001).
18. D.-L. Li, H.-S. Zhou and I. Honma, *Nature Mater*., **3**, 65 (2004).
19. Q.-Q. Wang and D.F. Shantz, *J. Solid State Chem*., **181**, 1659 (2008).
20. M. Guidotti, I. Batonneau-Gener, E. Gianotti, L. Marchese, S. Mignard, R. Psaro, M. Sgobba and N. Ravasio, *Micropor. Mesopor. Mater*., **111**, 39 (2008).
21. S. Angloher, J. Kecht and T. Bein, *Micropor. Mesopor. Mater*., **115**, 629 (2008).
22. Q.-D. Qin, J. Ma and K. Liu, *J. Hazard. Mater*., **162**, 133 (2009).
23. M. Lezanska, G.S. Szymanski, P. Pietrzyk, Z. Sojka and J.A. Lercher, *J. Phys. Chem. C*, **111**, 1830 (2007).
24. C.B. Murray, C.R. Kagan and M.G. Bawendi, *Ann. Rev. Mater. Sci*., **30**, 545 (2000).
25. T. Kodaira, T. Ikeda and H. Takeo, *Chem. Phys. Lett*., **300**, 499 (1999).
26. H.-P. He, Z.-Z. Ye and Y.-X. Wang, *J. Lumin*., **124**, 71 (2007).
27. L. Zhao, Y.-X. Wang, Z. Chen and Y.-M. Zou, *Physica B*, **403**, 1775 (2008).
28. M.I. Freedhoff, A.P. Marchetti and G.L. Mclendon, *J. Lumin*., **70**, 400 (1996).
29. T. Kodaira and T. Ikeda, *Mol. Cryst. Liq. Cryst*., **341**, 441 (2000).
30. S. Rodrigues, S. Uma, I.N. Martyanov and K.J. Klabunde, *J. Catal*., **233**, 405 (2005).
31. Y.J. Zang and R. Farnood, *J. Curr. Chem. Eng. Sci*., **64**, 2881 (2009).
32. Y. Tanamura, T. Uchida, N. Teramae, M. Kikuchi, K. Kusaba and Y. Onodera, *Nano. Lett*., **1**, 387 (2001).
33. M. Urban, Z. Konya, D. Mehn, J. Zhu and I. Kiricsi, *Phys. Chem. Commun*., **5**, 138 (2002).
34. H.R. Emamian, A. Honarbakhsh-raouf, A. Ataie and A. Yourdkhani, *J. Alloys. Comp*., **480**, 681 (2009).
35. D.B. Hamal and K.J. Klabunde, In Nanoscale Materials in Chemistry: Environmental Applications, (L. Erickson; ACS Symposium Series; American Chemical Society: Washington DC), Ch. 11, p. 191 (2010).
36. S. Rodrigues, S. Uma, I.N. Martyanov and K.J. Klabunde, *J. Catal*., **233**, 405 (2005).
37. Q. Cai, Z.-S. Luo, W.-Q. Pang, Y.-W. Fan, X.-H. Chen and F.-Z. Cui, *Chem. Mater*., **13**, 258 (2001).
38. J.C.P. Broekhoff and J.H. de Boer, *J. Catal*., **10**, 368 (1968).
39. S. Brumauer, P.H. Emmett and E. Teller, *J. Am. Chem. Soc*., **60**, 309 (1938).
40. E.P. Barett, L.G. Joyner and P.P. Halenda, *J. Am. Chem. Soc*., **73**, 373 (1951).
41. Q.-Z. Zhai, S.-L. Qiu, F.-S. Xiao, Z.-T. Zhang, C.-L. Shao and Y. Han, *Mater. Res. Bull*., **35**, 59 (2000).
42. S.-H. Chien, M.-C. Kuo and C.-L. Chen, *J. Chin. Chem. Soc*., **52**, 733 (2005).
43. S. Brunauer, L.S. Deming, W.S. Deming, W.E. Deming and E. Teller, *J. Am. Chem. Soc*., **62**, 1723 (1940).
44. K.S.W. Sing, D.H. Everett, R.A.W. Haul, L. Moscou, R.A. Pierotti, J. Rouquerol and T. Siemieniewska, *Pure Appl. Chem*., **57**, 603 (1985).
45. L. Vradman, M.V. Landau, D. Kantorovich, Y. Koltypin and A. Gedanken, *Micropor. Mesopor. Mater*., **79**, 307 (2005).
46. J.R. Agger, M.W. Anderson, M.E. Pemble, O. Terasaki and Y. Nozue, *J. Phys. Chem. B*, **102**, 3345 (1998).
47. T. Bein, *Chem. Mater*., **8**, 1636 (1996).
48. M.I. Freedhoff, A.P. Marchetti and G.L. Mclendon, *J. Lumin*., **70**, 400 (1996).
49. J.-Y. Kim, S.-H. Park and J.-S. Yu, *Opt. Mater*., **21**, 349 (2002).
50. J.-C. Tu, N. Li, Y. Chi, S.-N. Qu, C.-X. Wang, Q. Yuan, X.-T. Li and S.-L. Qiu, *Mater. Chem. Phys*., **118**, 273 (2009).
51. Y. Chi, N. Li, J.-C. Tu, Y.-J. Zhang, X.-T. Li and C.-L. Shao, *J. Lumin*., **130**, 512 (2010).
52. Y. Masumoto, T. Kawamura, T. Ohzeki and S. Urabe, *Phys. Rev. B*, **46**, 1827 (1992).
53. T. Takagahara and K. Takeda, *Phys. Rev. B*, **46**, 15578 (1992).
54. H. Vogelsang, H. Stolz and W. Osten, *J. Lumin*., **70**, 414 (1996).
55. M. Comor and J.M. Nedeljkovic, *Chem. Phys. Lett*., **299**, 233 (1999).
56. L.E. Brus, *J. Chem. Phys*., **80**, 4403 (1984).